

Measuring Form Factors and Structure Functions with CLAS

G.P. Gilfoyle
representing the CLAS Collaboration
Physics Department, University of Richmond
28 Westhampton Way
Richmond, VA 23173 USA

Proceedings of the third International Conference in High-Energy Physics: HEP MAD07,
27 Sep - 2 Oct 2007, Antananarivo, Madagascar.

Abstract

The physics program at the Thomas Jefferson National Accelerator Facility includes a strong effort to measure form factors and structure functions to probe the structure of hadronic matter, reveal the nature of confinement, and develop an understanding of atomic nuclei using quark-gluon degrees of freedom. The CLAS detector is a large acceptance device occupying one of the end stations. We discuss here two programs that use CLAS; measuring the magnetic form factor of the neutron, and the virtual photon asymmetry of the proton. The form factor has been measured with unprecedented kinematic coverage and precision up to $Q^2 = 4.7 \text{ GeV}^2$ and is consistent within 5%-10% of the dipole parameterization. The proton virtual photon asymmetry has been measured across a wide range in Bjorken x . The data exceed the $SU(6)$ -symmetric quark prediction and show evidence of a smooth approach to the scaling limit prescribed by perturbative QCD.

1 Introduction

The Thomas Jefferson National Accelerator Facility (Jefferson Lab or JLab) is the United States' newest national laboratory and is located in Newport News, VA. It is focused on mapping the geography of the transition from the successful hadronic model of atomic nuclei to one based on the underlying quark-gluon constituents of matter. The central instrument is the Continuous Electron Beam Accelerator Facility (CEBAF) which is a superconducting, linear, electron accelerator. About 1.4-km long and shaped like a racetrack, it can produce electron beams up to 6 GeV in energy with 80% polarization. Currents can vary from 1-50 nA. One of the accelerator end stations houses the CEBAF Large Acceptance Spectrometer (CLAS), a 35-ton, large-solid-angle device built around six superconducting coils that produce a toroidal magnetic field [1]. The CLAS consists of layers of drift chambers to measure charged particle trajectories, scintillators for timing measurements, Cerenkov counters to identify electrons, and electromagnetic calorimeters to measure energy. The focus of this paper is the measurement of form factors and structure functions with CLAS. Below we focus on two recent experiments in CLAS to measure the neutron magnetic form factor and the proton virtual photon asymmetry.

2 Magnetic Form Factor of the Neutron

The elastic form factors of the proton and neutron are fundamental quantities which have been studied for decades. The dominant features of the larger form factors G_M^p , G_E^p , and G_M^n were established in the 1960's: the dipole form $G_D = (1 + Q^2/0.71)^{-2}$ gave a good description within the experimental uncertainties, corresponding (at least for $Q^2 \ll 1 \text{ GeV}^2$) to an exponential falloff in the spatial densities of charge and magnetization. In the intervening decades, obtaining higher precision measurements of these quantities has been one thrust of the field, while new directions have also emerged, especially over the past decade. These include precise measurements of the neutron electric form factor [2], and extractions of the strange electric and magnetic form factors for the proton [3], as well as time-like form factors [4]. In addition to experimental progress, there has been renewed theoretical interest on several fronts [5]. First, models of the nucleon ground state can often be used to predict several of these quantities, and it has proven to be very difficult to describe all of the modern data simultaneously in a single model approach. Second, lattice calculations are now becoming feasible in the few-GeV² range, and over the next decade these calculations will become increasingly precise. Finally, since elastic form factors are a limiting case of the generalized parton distributions (GPDs), they can be used to constrain GPD models [6]. For this purpose, high precision and a large Q^2 coverage is important [6]. At present the neutron magnetic form factor at larger Q^2 is known much more poorly than the proton form factors.

The present measurement [8] makes use of quasielastic scattering on deuterium where final state protons and neutrons are detected. The ratio of ${}^2\text{H}(e, e'n)$ to ${}^2\text{H}(e, e'p)$ in quasi-free kinematics is approximately equal to the ratio of elastic scattering from the free neutron and proton. The ratio is:

$$R_D = \frac{\frac{d\sigma}{d\Omega}[{}^2\text{H}(e, e'n)_{\text{QE}}]}{\frac{d\sigma}{d\Omega}[{}^2\text{H}(e, e'p)_{\text{QE}}]} = a \cdot R_{free} = a \cdot \frac{\frac{(G_E^n)^2 + \tau(G_M^n)^2}{1+\tau} + 2\tau(G_M^n)^2 \tan^2(\frac{\theta}{2})}{\frac{(G_E^p)^2 + \tau(G_M^p)^2}{1+\tau} + 2\tau(G_M^p)^2 \tan^2(\frac{\theta}{2})} \quad (1)$$

where $\tau = Q^2/4M^2$, M is the nucleon mass, and θ is the electron scattering angle. Using deuteron models one can accurately compute the correction factor $a(Q^2, \theta_{pq})$, which is nearly unity for quasielastic kinematics and higher Q^2 . The value of G_M^n is then obtained from the measured value of R_D and the experimentally known values of G_E^n , G_M^p , and G_E^p . This method has been used previously [9]. The $(e, e'n)$ and $(e, e'p)$ reactions were measured in this work at the same time from the same target. Use of the ratio R_D under these circumstances reduces or eliminates several experimental uncertainties, such as those associated with the luminosity measurement or radiative corrections. The remaining major correction is for the detection efficiency of the neutron.

Neutrons were measured in two CLAS scintillator-based detectors: the forward-angle electromagnetic shower calorimeters and the time-of-flight (TOF) scintillators. The efficiency measurement was performed using tagged neutrons from the ${}^1\text{H}(e, e'\pi^+)X$ reaction where the mass of the final state M_X was chosen to be that of the neutron. Since the precise value of the detection efficiency can vary with time-dependent and rate-dependent quantities such as photomultiplier tube gain, the detection efficiency was measured *simultaneously* with the primary deuterium measurement. Two separate targets were positioned in the beam at the same time, one for deuterium and the other for hydrogen, separated by less than 5 cm. Plots of the resulting neutron detection efficiencies are shown in Fig. 1. The left-hand plot shows the results for the forward electromagnetic shower calorimeter, while the right-hand panel shows the results for the time of flight scintillators.

The CLAS extraction of $G_M^n(Q^2)$ actually consists of multiple overlapping measurements. The time of flight scintillators cover the full angular range of the spectrometer, while the forward

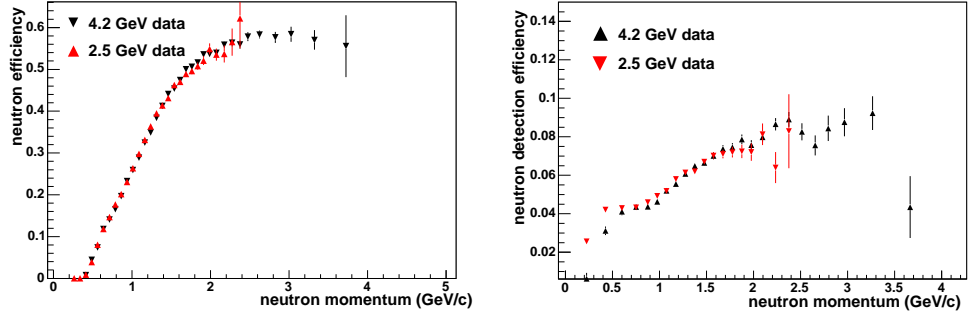


Figure 1: Detection efficiency versus momentum for neutrons detected in the forward-angle electromagnetic calorimeters at two different beam energies (left-hand panel) and in the TOF system (right-hand panel). The efficiency has been integrated over all six sectors of the CLAS.

calorimeters cover a subset of these angles, thus $G_M^n(Q^2)$ can be obtained from two independent measures of the neutron detection efficiency. In addition, the experiment was carried out with two different beam energies that had overlapping coverage in Q^2 , so that the detection of the protons of a given Q^2 took place in two different regions of the drift chambers. As a result, essentially four measurements of $G_M^n(Q^2)$ have been obtained from the CLAS data that could have four independent sets of systematic errors. Preliminary results are shown in Figure 2 of the reduced form factor $G_M^n/(\mu_n G_D)$ for the measurements. The four measurements are consistent within the statistical errors, suggesting that the systematic errors are well-controlled and small.

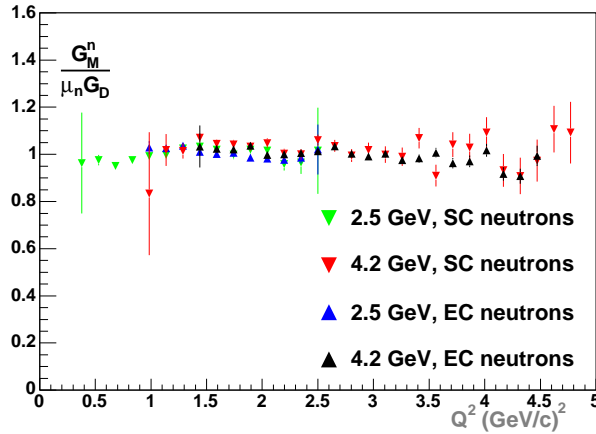


Figure 2: Preliminary results for $G_M^n/(\mu_n G_D)$ as a function of Q^2 for four different measurements. Uncertainties are statistical one only.

One of the goals of this experiment is to achieve a systematic uncertainty of 3% or less [7]. The biggest contributor to this uncertainty is the parameterization of the neutron detection efficiency, but there are significant contributions from the uncertainty in the other elastic form factors (recall Equation 1), and the effect of the Fermi motion in the deuteron. Details on the

determination of these uncertainties and other smaller ones can be found in Ref [8]. Here we discuss the analysis of the large contributors.

As described above the neutron detection efficiency in the calorimeters and the TOF system was measured simultaneously with the production data using tagged neutrons from the $p(e, e'\pi^+)n$ reaction. The results for both detector systems were fitted with a polynomial at low neutron momentum and a plateau at large momentum. The order of the polynomial and position of the plateau edge were varied to test the sensitivity of G_M^n as a function of Q^2 . Uncertainties in the range 1-2% were obtained. The uncertainties in the other elastic form factors contribute to the uncertainty in G_M^n (see Equation 1). The uncertainty in the proton cross section was estimated using the difference between two parameterizations by Bosted and Arrington [10, 11]. For the effect of G_E^n , the difference between the Galster parameterization and a fit by Lomon was used [12, 13]. These uncertainties had a maximum of 1.5% and were typically much less. The other large contributor was the effect of the Fermi motion in the deuteron knocking the scattered nucleons out of the CLAS acceptance. The effect was studied in a simulation using two dramatically different choices for the Fermi momentum distribution; a flat distribution and the Hulthen distribution. These two Fermi momentum distributions have very different effects on the neutron and proton spectra, but in the ratio we found the difference to be less than 1%. The complete inventory of uncertainties was combined in a weighted average of the systematic uncertainty as a function of Q^2 . The final uncertainty varied from 1.7-2.5% across the full Q^2 range of the data.

The preliminary results are shown in Fig. 3 together with a sample of existing data. The error bars shown on the points are due only to statistical uncertainties. The bar graph represents the systematic uncertainty as a function of Q^2 . The data shown are the weighted averages of the four overlapping individual measurements discussed above. A few features are noteworthy.

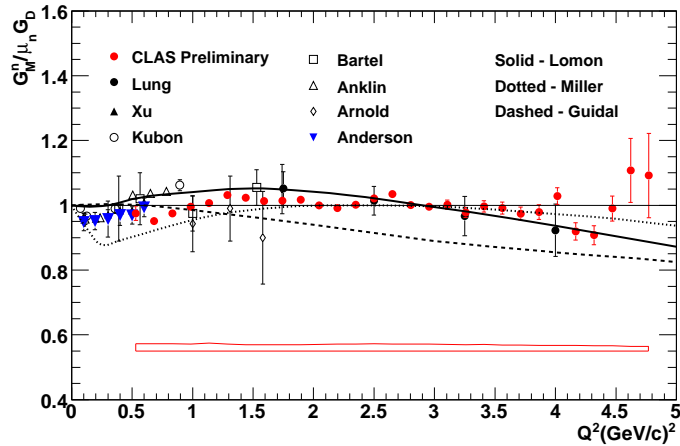


Figure 3: Preliminary results for $G_M^n/(\mu_n G_D)$ from CLAS are compared with a selection of previous data. See Ref [5] and references therein and Ref. [16]

First, the quality and coverage of the data is a very substantial improvement over the existing world's data set. Second, the dipole form appears to give a good representation of the data over the Q^2 range measured, which is at variance at higher Q^2 with parameterizations based

on previous data, which tend to show a more strongly decreasing trend for $G_M^n/(\mu_n G_D)$ with increasing Q^2 .

The curves shown in Figure 3 are from theoretical calculations by Lomon, Guidal, *et al.*, and Miller [13, 14, 15] using the world's data on the elastic form factors without the experimental results we report here. In the Lomon model the ρ , ω , ϕ , $\omega'(1419)$, and $\rho'(1450)$ vector meson pole contributions evolve at high momentum transfer to conform to the predictions of perturbative QCD. Recent data on the elastic nucleon form factors measured with polarization techniques is included in the sample. Excellent fits are obtained when older data on G_E^n and G_E^p inconsistent with the recent polarization results are excluded. In the work by Guidal, *et al.* a Regge parameterization of the generalized parton distribution (GPDs) is used to characterize the elastic nucleon form factors at low momentum transfer and then extended to higher momentum transfer. The calculation reproduces the more rapid drop observed in existing data at higher Q^2 , but is not consistent with the dipole approximation and our preliminary results. In the Miller work, the nucleon is treated using light-front dynamics as a relativistic system of three bound quarks and a surrounding pion cloud. The model achieves a good description of the existing nucleon form factors, but does not include the results here in the analysis.

3 Virtual Photon Asymmetry of the Proton

The spin structure of the nucleon has been investigated in a series of much-discussed polarized lepton scattering experiments over the last 25 years [17, 18, 19, 20, 21]. These measurements, most of which covered the deep inelastic scattering (DIS) region of large final-state invariant mass W and momentum transfer Q^2 , compared the Q^2 -dependence of the polarized structure function g_1 with perturbative QCD evolution equations and shed new light on the structure of the nucleon. Among the most surprising results was the realization that only a small fraction of the nucleon spin (20-30%) is carried by the quark helicities, in disagreement with quark model expectations of 60-75%. This reduction is often attributed to the effect of a negatively polarized quark sea at low momentum fraction x , which is typically not included in quark models (see the paper by Isgur [22] for a more detailed discussion).

For a more complete understanding of the quark structure of the nucleon, it is advantageous to concentrate on a kinematic region where the scattering is most likely to occur from a valence quark in the nucleon carrying more than a fraction $x = 1/3$ of the nucleon momentum. In particular, the virtual photon asymmetry, $A_1(x) \approx g_1(x)/F_1(x)$ (where F_1 is the usual unpolarized structure function) can be (approximately) interpreted in terms of the polarization $\Delta u/u$ and $\Delta d/d$ of the valence u and d quarks in the proton in this kinematic region, while the contribution from sea quarks is minimized. This asymmetry also has the advantage of showing only weak Q^2 -dependence [6,8], making a comparison with various theoretical models and predictions more straightforward.

In this Proceedings, we discuss the first high-precision measurement of $A_1(x, Q^2)$ for the proton and the deuteron at moderate to large x ($x \geq 0.15$) over a range of momentum transfers $Q^2 = 0.05$ -5.0 GeV², covering both the resonance and the deep inelastic region [17]. Longitudinally polarized electrons from CEBAF of several beam energies around 1.6 GeV and 5.7 GeV were scattered off longitudinally polarized ammonia targets ¹⁵NH₃ and ¹⁵ND₃ and detected in CLAS. The target material was kept in a 1 K liquid helium bath and was polarized via Dynamic Nuclear Polarization (DNP) [23]. The target polarization was monitored online using a Nuclear Magnetic Resonance (NMR) system. The beam polarization was measured at regular intervals with a Moeller polarimeter. The product of beam and target polarization ($P_b P_t$) was determined from the well-known asymmetry for elastic (quasielastic) scattering from polarized

protons (deuterons), measured simultaneously with inelastic scattering. For the 1.6 GeV data set, the average polarization product was $P_b P_t = 0.540 \pm 0.005$ (0.180 ± 0.007) for the $^{15}\text{NH}_3$ ($^{15}\text{ND}_3$) target. The corresponding values for the 5.7 GeV data set are 0.51 ± 0.01 and 0.19 ± 0.02 .

The data analysis proceeds along the following steps (see Refs. [17, 21] for more details). We first extract the raw count rate asymmetry $A_{\parallel}^{raw} = (N^+ N)/(N^+ + N)$, where the electron count rates for anti-parallel (N^+) and parallel (N) electron and target polarization are normalized to the (live-time gated) beam charge for each helicity. The background due to misidentified pions and electrons from decays into e^+e^- pairs (a few percent in all cases) has been subtracted from these rates. We divide the result by the product of beam and target polarization $P_b P_t$ and correct for the contribution from non-hydrogen nuclei in the target. For this purpose, we use auxiliary measurements on ^{12}C , ^4He and pure ^{15}N targets. We then combine the asymmetries for different beam and target polarization directions, thereby reducing any systematic errors from false asymmetries (no significant differences between the different polarization sets were found). Finally we apply radiative corrections using the code RCSLACPOL [24]. The (quasi-)elastic radiative tail contribution to the denominator of the asymmetry is treated as a further dilution factor.

The final result is the longitudinal (Born) asymmetry $A_{\parallel} = D(A_1 + \eta A_2)$, where the depolarization factor $D = (1 - E'\epsilon/E)/(1 + \epsilon R)$, E is the beam energy, E' is the scattered electron energy, $\epsilon = (2EE'Q^2/2)/(E^2 + E'^2 + Q^2/2)$ is the virtual photon polarization, $R < 0.2$ is the ratio of the longitudinal to the transverse photoabsorption cross section and $\eta = (\epsilon\sqrt{Q^2})/(EE'\epsilon)$. The asymmetry A_2 is the longitudinal-transverse interference virtual photon asymmetry. We use the standard notations for the energy transfer, $\nu = EE'$, and four-momentum transfer squared, $Q^2 = 4EE'\sin^2(\theta/2)$. A parameterization of the world's data was used to model A_2 and R and to extract A_1 [24, 25].

The results for $A_1(x)$, averaged over $Q^2 > 1 \text{ GeV}^2$ and $W > 2 \text{ GeV}$, are shown in Fig. 4 for the proton and the deuteron. At small x , where our average Q^2 is close to 1 GeV^2 , the

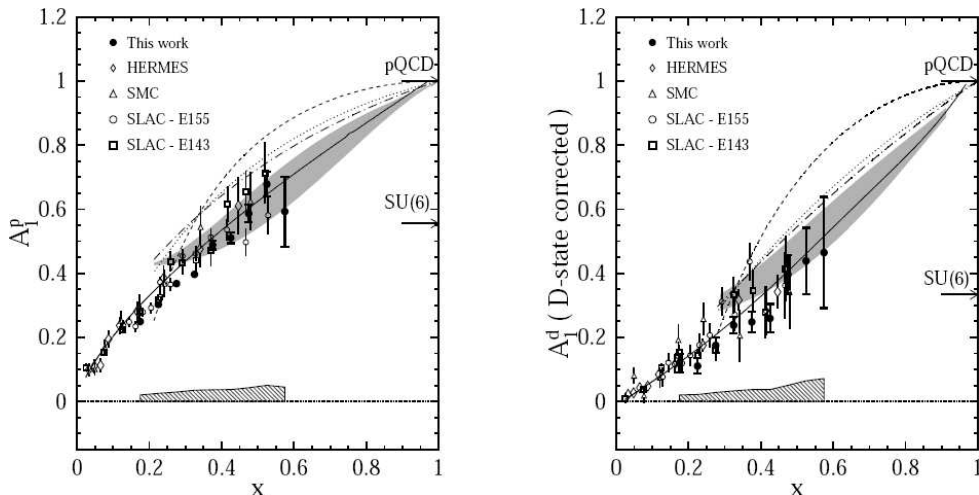


Figure 4: Results for the asymmetry $A_1(x)$ for protons (left-hand panel) and deuterons (right-hand panel) [17]. The $SU(6)$ expectation is shown by the arrow in each panel.

data fall below our parametrization of the world data with $Q^2 = 10 \text{ GeV}^2$ (solid line). This deviation is due to the Q^2 -dependence shown in Ref[17]. In contrast, all data points for the

proton and the deuteron lie above the SU(6) values for $x > 0.45$. The hyperfine interaction model of SU(6) symmetry breaking by Isgur [22] (grey band in figures) is closest to the data. Of the different mechanisms for SU(6) symmetry breaking considered by Close and Melnitchouk [26], the model with suppression of the symmetric quark wave function (dot-dashed curve in Fig 4) deviates least from the data. The dashed curve is for a model using helicity-1/2 dominance and the dotted one is for spin-1/2 dominance. In general, our results are in better agreement with models (like the first two mentioned above) in which the ratio of down to up quarks, d/u , goes to zero and the polarization of down quarks, $\Delta d/d$ tends to stay negative for rather large values of x , in contrast to the behavior expected from hadron helicity conservation.

Within a naive quark - parton model (and ignoring any contribution from strange quarks), we can estimate the quark (plus antiquark) polarizations $\Delta u/u$ and $\Delta d/d$ directly from our data by combining the results for g_1 from the proton and the deuteron (including some nuclear corrections for the deuteron D-state and Fermi motion) with our parametrization of the world data on F_1^p and F_1^d . The result shown in Figure 5 has relatively large statistical errors for $\Delta d/d$, since neither A_1^p nor A_1^d are very sensitive to $\Delta d/d$. Included are all data above $W = 1.77$ GeV

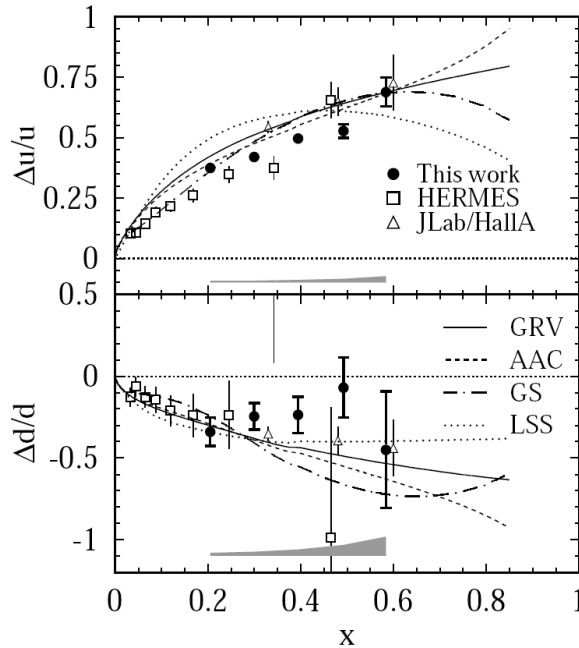


Figure 5: Quark polarizations $\Delta u/u$ (upper panel) and $\Delta d/d$ (lower panel) extracted from the asymmetry data [17].

and $Q^2 = 1$ GeV². Also shown are semi-inclusive results from HERMES [27] and inclusive results from Hall A data [11] combined with previous data from CLAS [20]. The solid line is from the leading order fit to the world data by GRSV [28], the dashed line is from the AAC fit [29], the dash-dotted line is from Gehrmann and Stirling [30] and the dotted line indicates the latest fit from LSS [31] which includes higher twist corrections. Our estimate is consistent with the result from the ³He experiment [19], showing no indication of a sign change to positive values up to $x \approx 0.6$. At the same time, these data for $\Delta u/u$ show a consistent increase with x ,

compatible with $\Delta u/u \rightarrow 1$ as $x \rightarrow 1$. Our data are also in reasonable agreement with existing leading order perturbative QCD fits.

4 The Future

The future of the study of form factors and structure functions at JLab. As part of the 6-GeV program at JLab analysis continues on a low- Q^2 measurement of the magnetic form factor of the neutron and in other areas like the transition form factors which probe the structure of the excited states of the nucleon. New exit channels are under investigation to extract the structure functions. More importantly, both the study of structure functions and form factors will be an essential component of the 12-GeV Upgrade at JLab. This new project will double the current energy of CEBAF, add a new experimental hall to focus on the discovery of exotic mesons, and upgrade the other three, existing halls to take advantage of the new physics opportunities. CLAS will be replaced by a new detector CLAS12 which will be able to operate at a luminosity ten times greater than the current device. The scientific motivation for measuring the magnetic form factor of the neutron and the virtual photon asymmetry is strongly made in the Conceptual Design Report [32]. In fact, two experiments to measure $A_1(x)$ (PR12-06-109) and G_M^n (PR12-07-104) have been approved in the last eighteen months by the JLab Program Advisory Committee for running during the first five years of the Upgrade [33, 34].

References

- [1] B. Mecking, *et al.*, Nucl. Instr. and Meth. A **503/3**, 513 (2003).
- [2] R. Madey *et al.*, Phys. Rev. Lett. **91**, 122002 (2003).
- [3] K. A. Aniol *et al.* (HAPPEX Collaboration), Phys. Lett. **B635**, 275 (2006).
- [4] F. Iachello, Q. Wan, Phys. Rev. C, **69**, 055204 (2004).
- [5] C.E. Hyde-Wright and K.deJager, Ann. Rev. Nucl. Part. Sci. **54**, 217 (2004).
- [6] M. Diehl, Th. Feldmann, R. Jakob, and P. Kroll, Eur.Phys.J.C **39**, 1 (2005).
- [7] W. Brooks and M.F. Vineyard, *The Neutron Magnetic Form Factor from Precision Measurements of the Ratio of Quasielastic Electron-Neutron to Electron-Proton Scattering in Deuterium*, Jefferson Lab Experiment E94-017 1994.
- [8] J.D. Lachniet, *A High Precision Measurement of the Neutron Magnetic Form Factor Using the CLAS Detector*, thesis, Carnegie Mellon University.
- [9] G. Kubon, *et al.*, Phys.Lett. **B524**, 26-32 (2002).
- [10] P. Bosted, Phys. Rev. C **51**, 409 (1995).
- [11] J. Arrington, private communication.
- [12] S. Galster, H. Klein, J. Moritz, K.H. Schmidt, D. Wegener, and J. Blechwenn, Nucl. Phys. **B32**, 221 (1971).
- [13] E. Lomon, Phys. Rev. C **66**, 045501 (2002).

- [14] M. Guidal, M.V.Polyakov, A. V. Radyushkin, and M.Vanderhaeghen, Phys. Rev. D **58**, 054013 (2005).
- [15] G. Miller, Phys. Rev. C **66**, 032201(R) (2002).
- [16] B. Anderson, *et al.*, (Jefferson Lab E95-001 Collaboration), Phys.Rev.C **75**, 034003 (2007).
- [17] K.V. Dharmawardane, *et al.*, Phys. Lett. B, **641**, 11 (2006) and references therein.
- [18] M. Amarian, *et al.*, Jefferson Lab E94-010 Collaboration, Phys. Rev. Lett. **92** 022301 (2004).
- [19] X. Zheng, *et al.*, Jefferson Lab Hall A Collaboration, Phys. Rev. C **70** 065207 (2004).
- [20] R. Fatemi, *et al.*, CLAS Collaboration, Phys. Rev. Lett. **91** 222002 (2003).
- [21] J. Yun, *et al.*, CLAS Collaboration, Phys. Rev. C **67** 055204 (2003).
- [22] N. Isgur, Phys. Rev. D **59** 034013 (1999).
- [23] C.D. Keith, *et al.*, Nucl. Instrum. Methods A **501** 327 (2003).
- [24] K. Abe, *et al.*, E143 Collaboration, Phys. Rev. D **58** 112003 (1998).
- [25] P.L. Anthony, *et al.*, E155 Collaboration, Phys. Lett. B **493** 19 (2000).
- [26] F.E. Close, W. Melnitchouk, Phys. Rev. C **68** 035210 (2003).
- [27] A. Airapetian, *et al.*, HERMES Collaboration, Phys. Rev. D **71** (2005) 012003.
- [28] M. Glck, E. Reya, M. Stratmann, W. Vogelsang, Phys. Rev. D **63** (2001) 094005.
- [29] Y. Goto, *et al.*, Asymmetry Analysis Collaboration, Phys. Rev. D **62** (2000) 034017.
- [30] T. Gehrmann, W.J. Stirling, Phys. Rev. D **53** (1996) 6100.
- [31] E. Leader, A.V. Sidorov, D.B. Stamenov, Phys. Rev. D **73** (2006) 034023.
- [32] Conceptual Design Report (CDR) for The Science and Experimental Equipment for The 12 GeV Upgrade of CEBAF, Thomas Jefferson National Accelerator Laboratory, March 25, 2005.
- [33] Program Advisory Committee Report (PAC30), Thomas Jefferson National Accelerator Laboratory, October 18, 2006.
- [34] Program Advisory Committee Report (PAC32), Thomas Jefferson National Accelerator Laboratory, October 18, 2007.